Nanoscale

PAPER

View Article Online
View Journal | View Issue



Cite this: *Nanoscale*, 2018, **10**, 8600

# Plasmon-induced nonlinear response of silver atomic chains†

Lei Yan, Mengxue Guan and Sheng Meng *

Received 13th March 2018,
Accepted 9th April 2018

DOI: 10.1039/c8nr02086h

rsc.li/nanoscale

Nonlinear response of a linear silver atomic chain upon ultrafast laser excitation has been studied in real time using the time-dependent density functional theory. We observe the presence of nonlinear responses up to the fifth order in tunneling current, which is ascribed to the excitation of high-energy electrons generated by Landau damping of plasmons. The nonlinear effect is enhanced after adsorption of polar molecules such as water due to the enhanced damping rates during plasmon decay. Increasing the length of atomic chains also increases the nonlinear response, favoring higher-order plasmon excitation. These findings offer new insights towards a complete understanding and ultimate control of plasmon-induced nonlinear phenomena to atomic precision.



## 1. Introduction

Boosting nonlinear optical and electronic effects at the nanoscale is an important subject of extensive theoretical and experimental studies. Since the photon–photon interaction is intrinsically weak, nonlinear effects can be generated only with very high light intensities before significant material damage occurs, limiting the choice of materials.[1] A promising route for circumventing this difficulty and achieving efficient nonlinear responses is to strengthen the localized optical field through the excitation of localized surface plasmon resonance (LSPR). LSPR can be exploited to dramatically enhance light–matter interaction, enabling nonlinear effects observable with low incident light intensity.[2,3] LSPR exhibits extraordinary properties including extended lifetime, ultrafast dynamics, and easy tunability through the choice of materials, dielectric environment, and specific size and shape of nanostructures.[4–6] Various noble metal nanostructures can be used to accommodate LSPR. Among these materials, prototype structures such as linear atomic chains, which can be assembled with a scanning tunneling microscope (STM),[7,8] have attracted intensive attention. The size and shape of such structures are tunable down to the precision of a single atom.[7,8] Collective electronic oscillation at such a scale is a fundamental subject of its own interest.[9,10]

Nonlinear plasmonics is a fast-growing field of research due to its potential applications in energy,[11] optoelectronic devices,[12] and biological imaging and sensing.[13] LSPR can boost nonlinear optical effects by tuning the shape of the nanostructures such as non-centrosymmetric gold nanocup[14] for enhanced second-harmonic generation (SHG) and gold bowtie antenna[15] for third-harmonic generation (THG). Plasmon can also respond on the timescale of a few femtoseconds,[16] favoring the appearance of specific nonlinear processes *via* electron bouncing and rescattering. Recently, Kravtsov *et al.* demonstrated plasmon-enhanced four-wave mixing (FWM) on a gold tip by femtosecond near-field imaging.[17] However, fundamental understanding of the nonlinear response associated with plasmon excitation, especially quantum and nonlocal effects on the scale of a single atom, is still lacking.

For the systems with a size of tens of nanometers, classical methods such as the finite-difference time-domain (FDTD) approach based on the Drude model and Maxwell equations can yield accurate plasmonic modes.[18] However, when the system sizes further shrink to a few nanometers, the classical approaches fail due to the lack of nonlocal responses in the dielectric function and interband transitions.[19] In this case, classical approaches may overestimate field enhancement[20] and produce smaller resonant energy.[21] In such small systems, quantum mechanical descriptions such as time-dependent density functional theory (TDDFT) have become necessary.

Rigorous TDDFT calculations for nanoparticles (NPs) show low-order (up to 2–3 orders) nonlinear oscillations at the plasmon frequency.[3,11,22,23–28] Higher order (>3) nonlinear responses are rarely reported. In addition, only few studies reveal nonlinear effects in terms of the electron tunneling current between NP and a nearby molecule, which is important for plasmon-driven photocatalysis. Moreover, questions of how these high-frequency currents couple to molecular excitations, how to enhance the nonlinear responses, and the origin of plasmon-induced nonlinearity remain to be

*Beijing National Laboratory for Condensed Matter Physics and Institute of Physics, Chinese Academy of Sciences, Beijing 100190, China. E-mail: smeng@iphy.ac.cn*

†Electronic supplementary information (ESI) available. See DOI: 10.1039/c8nr02086h

explored.[29] Herein, we report high-order nonlinear responses in the tunneling current spectra and reveal their atomistic mechanisms.

Herein, we investigate the nonlinear response of a model plasmonic system, a linear silver chain coupled to molecules, using *ab initio* TDDFT. The spectra of tunneling currents upon femtosecond laser excitation have been analyzed, which show features of double and high-order excitations. Upon adsorption of polar molecules such as water, the nonlinear response is dramatically enhanced. We further demonstrate that this enhancement results from faster decay of plasmons in the presence of adsorbed molecules. More importantly, we observe the nonlinear response up to the fifth order in the current spectrum, and we ascribe it to hot electron generation as a consequence of ultrafast plasmon decay. Increasing the length of the silver chain increases the nonlinear response, generating higher-order plasmon modes. This study provides a theoretical basis for understanding the microscopic mechanism of plasmon-induced nonlinear response and achieving ultimate control at the atomic scale.

## 2. Computational methods

First-principles calculations have been performed with the real-space TDDFT code OCTOPUS[30] using Adiabatic Local Density Approximation (ALDA) for the exchange correlation functional. The simulation zone is defined by assigning a sphere of radius 6.0 Å around each atom. The electronic wave functions are represented on a uniform mesh inside the simulation zone with a spacing of 0.2 Å between the grid points. Charge transfer is estimated by integrating the total charge density in a sphere with a radius of 4.5 Å around a water molecule. Hartwigsen–Goedecker–Hutter[31] pseudopotentials are used to represent the interaction between valence electrons and the atomic core. Spectra of photoabsorption and tunneling current are obtained by propagating the electronic density for 40 000 steps with a time step of 0.002 fs following an impulse excitation $E(t) = E_0\delta(t)$ and Gaussian wavepackets of laser pulses.

In our simulations, Ag atoms in the chain are frozen, and an interatomic distance of 2.89 Å is chosen from the experimental value for Ag chains on NiAl(110) surface.[32] We select the Ag chain with $N = 6$ atoms as an example. Such a chain can be created by manipulating single Ag atoms on the NiAl(110) surface with a STM tip.[32] After geometry relaxation, the configuration of $H_2O$ adsorbed on the silver atomic chain with Ag–O distance of 2.43 Å is shown in Fig. 1(a).

## 3. Results and discussion

We first explore the optical absorption of the silver chain with a water molecule ($Ag_6H_2O$) induced by an impulse field with different intensities, as shown in Fig. 1(a). The absorption spectrum is dominated by Mie resonance at ~1.7 eV. For linear

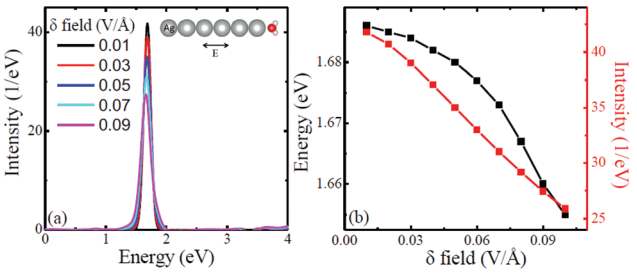


**Fig. 1** (a) Absorption spectrum of a linear $Ag_6$ chain with adsorbed water molecule induced by an impulse field with intensity $E_0$ = 0.01, 0.03, 0.05, 0.07, 0.09 V Å$^{-1}$. (b) Changes in peak energy and intensity in the absorption spectra with varying laser intensity.

sodium chains with $N$ = 1–18 atoms, the plasmon energy calculated by TDDFT is well-fitted with Mie frequencies calculated using the ellipsoidal jellium model.[33] We identify the analogous resonance at ~1.7 eV as a Mie resonance. After increasing the field strength, $E_0$, the width of absorption spectra increases, and the absorption intensity per unit field strength decreases, implying the breakdown of linear response. The intensity of the major absorption peak decreases from 42 to 26 eV$^{-1}$ for $E_0$ = 0.01–0.10 V Å$^{-1}$. The corresponding full width at half maximum value (FWHM) increases from 0.14 eV to 0.19 eV (Fig. S1†), whereas the oscillator strength remains almost constant (6.05–6.12). Meanwhile, the resonance energy also redshifts from 1.69 to 1.66 eV for $E_0$ = 0.01–0.10 V Å$^{-1}$ (Fig. 1(b)). In contrast, for the isolated silver chain $Ag_6$, the variation in absorption intensity with an increase in $E_0$ is much less than that for $Ag_6H_2O$, and FWHM exhibits almost no change (Fig. S1†). The charge transfer around the water molecule increases from 0.03 to 0.14$e$ with $E_0$ varying from 0.01 to 0.10 V Å$^{-1}$. This means that more electrons are transferred from the silver chain to the water molecule, leading to broadening and redshifting of the plasmon excitation peak.[34] Meanwhile, the increased FWHM value indicates faster dephasing of the plasmon.[35] Thus, these changes in the absorption spectrum suggest that electron transfer processes result in stronger dephasing of the plasmon excitation, which is similar to the results observed in the case of gold nanorods on graphene.[36]

To illustrate how charge transfer affects plasmon excitation processes, we display the response in tunneling currents induced by the impulse field (Fig. 2). The current $I_t$ is collected at the central plane between the end atom of the silver chain and water molecule in $Ag_6H_2O$, and it is at the same position for the isolated chain $Ag_6$. The variation in the current can be related to experimentally measurable quantities such as emission of high-energy photoelectrons or localized high harmonic generation.[37,38] The current localized at the end of the chain $Ag_6$ shows resonance at the Mie frequency $\omega$ = 1.67 eV, and its intensity increases linearly from 0.13 mA to 1.35 mA for $E_0$ = 0.01–0.10 V Å$^{-1}$ (Fig. 2(a)). The primary plasmon excitation characterizes the collective oscillation of many electrons in the system.

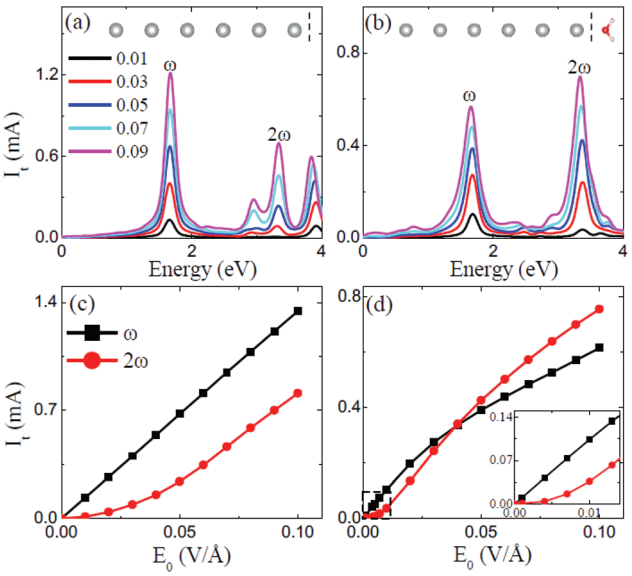


Fig. 2 Evolution of tunneling current spectrum with respect to laser intensity ($E_0$ = 0.01, 0.03, 0.05, 0.07, and 0.09 V Å$^{-1}$) during impulse excitation (a) at the end of silver chain $Ag_6$ and (b) in the gap between the silver chain and water molecule in $Ag_6H_2O$. Field intensity dependences of the two dominant peaks at Mie resonance $\omega$ and double excitation $2\omega$ for (c) $Ag_6$ and (d) $Ag_6H_2O$. The inset in panel (d) is a zoomed-in plot corresponding to the boxed area.

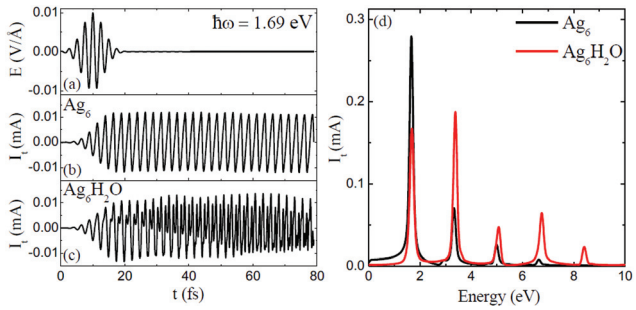


Fig. 3 Time evolution of the applied laser field (a) and tunnel currents for $Ag_6$ (b) and $Ag_6H_2O$ (c). The maximum laser intensity $E_{max}$ is 0.01 V Å$^{-1}$ with a resonant frequency of 1.69 eV. (d) Corresponding tunneling current spectra for $Ag_6$ and $Ag_6H_2O$.

In addition to Mie resonance at 1.67 eV, there is a second peak at 3.34 eV, and the energy of this peak is exactly twice the primary excitation energy. This local mode corresponds to SHG in the outgoing radiation. The intensity of the double excitation increases from 0.01 mA to 0.81 mA, following a quadratic relationship with laser intensity $E_0$ (Fig. 2(c)), indicating that it is induced by a two-step process.[29] Tunneling current in primary excitation is always higher than that in the second-order response for the isolated silver chain.

When adsorbing a water molecule at the end of the silver chain, the tunneling current displays both plasmon resonance and double excitations, as shown in Fig. 2(b). For weak laser intensities below 0.015 V Å$^{-1}$, the current for Mie resonance increases linearly, and the current for double excitation increases quadratically with the increasing field strength $E_0$. This trend is very close to that observed in the case of $Ag_6$. However, for strong laser fields beyond 0.015 V Å$^{-1}$, the current for the primary plasmon mode obviously diverges from linear behavior. The current for double excitation increases abruptly, and its contribution even exceeds that for primary Mie resonance for $E_0$ > 0.04 V Å$^{-1}$ (Fig. 2(d)). This can be ascribed to the excitation of hot electrons, which experience a lower tunneling barrier.[22] Therefore, with a water molecule adsorbed, a transition from linear response to nonlinear regime is observed at a critical field strength of 0.04 V Å$^{-1}$.

To better understand the effect of the adsorbed molecule on plasmon-induced nonlinear response, we directly analyze the tunneling current with ultrafast femtosecond laser pulses, as displayed in Fig. 3. The laser field polarized along the chain direction is shaped as a Gaussian wave packet,

$$E(t) = E_{max} \exp[-(t - t_0)^2/2\tau^2]\cos(\omega t - \omega t_0),$$

Here, the width $\tau$ is 3.3 fs, and $\omega$ is set to the plasmon resonance frequency 1.69 eV (see Fig. 3(a)). The laser field value reaches the maximum intensity $E_{max}$ = 0.01 V Å$^{-1}$ at time $t_0$ = 10 fs. Similar few-cycle pulses have been widely applied experimentally to engineer electronic excitations and ultrafast dynamics in gases and solids.[39]

In the isolated silver chain $Ag_6$, the tunneling current coherently oscillates following the external field, and it continues to increase before $t$ = 20 fs (Fig. 3(b)). After field attenuation at $t$ = 20 fs, the current continues to oscillate and shows negligible decay. With a water molecule adsorbed, the tunneling current exhibits phase shifts in the oscillations and shows the emergence of high-frequency modulation. The high-frequency modulation becomes more obvious as time progresses (Fig. 3(c)).

We display the spectra of tunneling current obtained by the Fourier transform of its time evolution (Fig. 3(d)). We find that in addition to Mie resonance and SHG, the third, fourth, and fifth-order excitations emerge for $Ag_6H_2O$. The SHG peak is even stronger than that for Mie resonance. In contrast, for the isolated silver chain $Ag_6$, Mie resonance dominates the spectrum, and nonlinear responses are weaker than those for $Ag_6H_2O$. Adsorbing a water molecule at the end of the silver chain greatly enhances the nonlinear responses.

To gain a deeper insight into plasmon-induced nonlinear responses, we analyze the time-evolved occupation of Kohn–Sham (KS) states, calculated by projecting time-dependent KS states onto the ground state. For $Ag_6$, the occupation of the lowest unoccupied molecular orbital (LUMO) oscillates coherently and increases to 0.06 (*i.e.*, ~0.12*e*) before $t$ = 20 fs (Fig. 4(a)). After the laser field falls off at $t$ = 20 fs, the occupation continuously oscillates without decay. Other virtual orbitals have low occupation. Upon water adsorption, the occupation of LUMO increases to 0.055 (*i.e.*, ~0.11*e*) before $t$ = 20 fs. Surprisingly, with laser field attenuation, the occupation

 

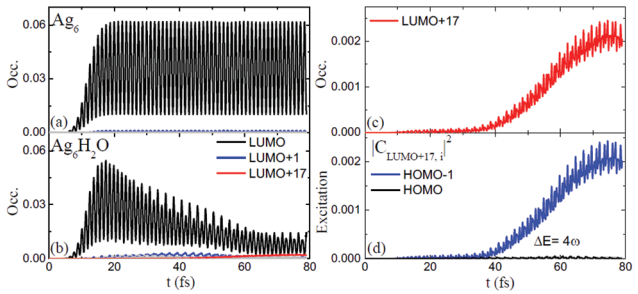


**Fig. 4** Time-evolved occupation of initially unoccupied Kohn–Sham states in (a) $Ag_6$ and (b) $Ag_6H_2O$ driven by a laser pulse shown in Fig. 3(a). (c) Zoomed-in plot for the occupation of the LUMO+17 state shown in panel (b). (d) Corresponding time-dependent transition coefficient $|C_{LUMO+17,\ i}|^2$ from all occupied states $i$ to the LUMO+17 state for $Ag_6H_2O$.

starts to decline and reaches 0.015 (*i.e.*, ~0.03*e*) at $t$ = 80 fs (Fig. 4(b)), which is very different from the results observed in the case of $Ag_6$. Thus, water adsorption at the end of the silver chain greatly accelerates plasmon decay.

The occupation of LUMO decreases exponentially (Fig. 4(b)), resulting in the excitation of high-energy electrons. Therefore, this plasmon decay of the silver chain into high-energy electron–hole pairs is identified as nonradiative Landau damping.[40] From $t$ = 20 fs to $t$ = 80 fs, the number of electrons on the LUMO orbital (calculated by projecting the time-dependent Kohn–Sham orbitals to adiabatic eigenstates) is decreased by 0.08*e*. That is, the number of high-energy hot electrons generated by the plasmon decay after a single laser pulse illumination is about 0.08*e* within ~60 fs.

In addition, the occupations of a few high-energy orbitals of $Ag_6H_2O$, particularly the LUMO+17 state, also change significantly. Before $t$ = 40 fs, the occupation of LUMO+17 is almost zero (Fig. 4(c)). After that, the occupation increases drastically to 0.002 at $t$ = 80 fs. We further display in Fig. 4(d) the transition coefficients $|C_{LUMO+17,i}|^2$. The coefficients are defined as time-dependent occupied KS orbitals $|i(t)\rangle$ projected onto the initial LUMO+17 state. The transition mainly comes from the HOMO−1 state, showing a gradual increase in transition coefficient after $t$ = 40 fs. This observation suggests the generation of hot electrons promoted from HOMO−1 to LUMO+17 by Landau damping of plasmon.[41] The KS level difference between HOMO−1 and LUMO+17 is 6.70 eV, which is approximately four times the incident laser frequency (1.69 eV). We infer that the fourth-order nonlinear response results from electron transitions from HOMO−1 to LUMO+17 through Landau damping during plasmon decay. Other nonlinear responses including SHG and THG have similar origins.

We then explore the laser intensity dependence of nonlinear responses (Fig. S2†). For laser intensity $E_{max}$ below 0.003 V Å$^{-1}$, the tunneling currents increase linearly, quadratically, trebly, and quadruply with an increase in $E_{max}$ for the first, second, third, and fourth-order responses, respectively. However, for stronger laser fields, the trend obviously diverges from linear response behaviors, similar to that observed in the case shown in Fig. 2(d). Furthermore, laser frequency dependence compares well with the overall shape of the optical absorption spectrum (Fig. S2†), which confirms that the nonlinear effect of tunneling current results from plasmon-induced hot electrons. If we replace water with a CO molecule, which has a tiny dipole moment of 0.12 Debye, the nonlinear responses significantly decrease (Fig. S3†). Therefore, the nonlinear response of the silver chain can be easily tuned by adjusting laser parameters and adsorption environment.

We also explore the dependence of tunneling current on the length of the atomic chain, as shown in Fig. 5(a). For silver chains with varying number of atoms $N$ = 4, 6, 8, 10, and 12, the resonant energies redshift and Mie resonances decrease from 0.18 mA to 0.13, 0.11, 0.09, 0.08 mA, respectively, as $N$ increases from 4 to 12. For the chains with $N$ = 4 and 6, there exist responses up to the second-order in the tunneling current spectrum. For $N$ = 8 and 10, a third-order response also appears. For $N$ = 12, fourth- and even fifth-order responses are observed. Therefore, increasing the length of the silver chain enhances nonlinear plasmon responses.

In addition, we analyze induced charge densities for peaks in the tunnel current spectra of $Ag_{12}$ as shown in Fig. 5(b). In our simulations, we utilize the impulse excitation along the chain to obtain the resonance peak in the absorption spectrum (see Fig. 1), and the energy of this peak corresponds to that of a first-order peak in the tunneling current spectrum. The nature of the resonance can also be reflected by the induced charge density at the resonance frequency, as shown in Fig. 5(b). For $n$ = 1 in $Ag_{12}$, the density response is asymmetric across the chain with its maximum at one end and minimum at the other, which shows the dipolar character of the plasmon oscillation. Along the chains, the difference in density envelope is monotonic for the $n$ = 1 mode, but exhibits oscillatory structures for $n$ = 2 and 3 modes (Fig. 5(b)) with $n$ oscillation periods, which results from the longitudinal quantization of plasmon in one dimension.[33] Fig. 4(b) also shows unambiguously the presence of multiple electronic excitations excluding single electron–hole excitation and reveals the collective nature of plasmons. More details are described in ref.

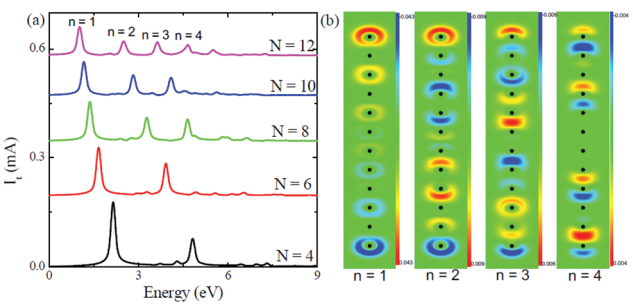


**Fig. 5** (a) Tunneling current spectra of linear silver chains with varying number of atoms ($N$ = 4, 6, 8, 10, and 12). Laser field strength: $E_0$ = 0.05 V Å$^{-1}$. (b) Fourier transform of time-evolved charge densities projected in the atomic plane at four peak frequencies $n$ = 1, 2, 3, and 4 for the chain $Ag_{12}$.

10 and 33. Clearly, for the peaks where $n$ = 1, 2, 3, and 4, the charge densities display first, second, third, and fourth order charge transfer patterns of dipolar plasmonic excitation, respectively. Therefore, we conclude that the nonlinear responses in the tunneling currents of silver chains are related to multiple-order plasmon excitations.

Due to the stringent requirements for computational resources in large-scale TDDFT calculations, we could only simulate up to a few tens of atoms as model systems, rather than large nanoparticles comprising millions of atoms used in typical experiments. We note that the LSPR response was dependent on the particle size. However, many conceptual models in TDDFT could produce the same phenomenon and explain puzzles in the experiments.[10,18,22,41–43] For example, using TDDFT, Yan *et al.*[10] studied LSPR of linear sodium chains with $N$ = 1–18 atoms, and they revealed the nature of transverse plasmonic mode observed in experiments. By employing TDDFT, Lauchner *et al.*[43] demonstrated the existence of molecular plasmon resonances in electrically doped materials, which were in excellent agreement with results from experiments. In this sense, the basic effect (high-order nonlinearities) can also be studied using cheaper approaches, which may be applied to more realistic systems as long as the quantum effects of electrons are included. We infer that the effect shown in Fig. 5(a) would persist in experimentally relevant system sizes and also, evidences from future experiments are desired. We thereby believe that the results presented herein provide implications on plasmon-induced nonlinearity, which is helpful for future experiments on similar and larger nanoparticles.

## 4. Conclusions

In conclusion, we have investigated the nonlinear response in the current spectra of silver atomic chains using TDDFT. We demonstrate that the nonlinear effect results from the high-energy hot electrons generated by plasmon decay. The nonlinear response is greatly enhanced with the adsorption of polar molecules such as water, due to faster Landau damping. When coupled with polar molecules, plasmons can decay to hot electrons within ~50 fs, which is responsible for the high-order nonlinear effects in tunneling currents. This relaxation pathway needs to be further justified in future experiments using similar and larger sized nanoparticles. In addition, increasing the length of silver chain also enhances the plasmon-mediated nonlinear effects. Our results shed light on the atomistic mechanisms regarding how hot electrons generated by plasmon decay contribute to nonlinear responses. This new knowledge provides a theoretical basis for understanding plasmon-induced catalysis and integrated nanophotonics. At the fundamental level, the coupled plasmon-molecule system, as a unique model, reveals relaxation pathways of collective excitations to the localized molecular state, which is a general and open issue in the field of quantum dissipation. On the practical side, adjusting the sizes of plasmonic nanosystems, laser parameters, and adsorption environments can greatly tune plasmon-induced nonlinear responses, offering possible paths for the ultimate control of plasmon-induced nonlinear phenomena to atomic precision. We expect that such insights into the fundamental plasmon-molecule coupling mechanism and the possibility of tuning the nonlinear response of LSPR are generally applicable to all plasmonic nanostructures and not limited to the model systems considered herein.

## Conflicts of interest

There are no conflicts to declare.

## Acknowledgements

We acknowledge helpful discussions with S. W. Gao and financial support from MOST (Grant No. 2016YFA0300902 and 2015CB921001), NSFC (Grant No. 11474328 and 11290164), and "Strategic Priority Research Program B" of the CAS (No. XDB070301).

## References

1 G. Grinblat, Y. Li, M. P. Nielsen, R. F. Oulton and S. A. Maier, *Nano Lett.*, 2016, **16**, 4635.
2 M. B. Mohamed, V. Volkov, S. Link and M. A. El-Sayed, *Chem. Phys. Lett.*, 2000, **317**, 517.
3 M. Kauranen and A. V. Zayats, *Nat. Photonics*, 2012, **6**, 737.
4 S. Link, M. B. Mohamed and M. A. El-Sayed, *J. Phys. Chem. B*, 1999, **103**, 3073.
5 P. K. Jain, K. S. Lee, I. H. El-Sayed and M. A. El-Sayed, *J. Phys. Chem. B*, 2006, **110**, 7238.
6 W. Ni, X. Kou, Z. Yang and J. Wang, *ACS Nano*, 2008, **2**, 677.
7 N. Nilius, T. M. Wallis and W. Ho, *Science*, 2002, **297**, 1853.
8 T. M. Wallis, N. Nilius and W. Ho, *Phys. Rev. Lett.*, 2002, **89**, 236802.
9 L. Yan, Z. Ding, P. Song, F. Wang and S. Meng, *Appl. Phys. Lett.*, 2015, **107**, 083102.
10 J. Yan, Z. Yuan and S. Gao, *Phys. Rev. Lett.*, 2007, **98**, 216602.
11 P. Narang, R. Sundararaman, A. S. Jermyn, W. A. Goddard and H. A. Atwater, *J. Phys. Chem. C*, 2016, **120**, 21056.
12 W. Van Sark, J. de Wild, J. K. Rath, A. Meijerink and R. E. I. Schropp, *Nanoscale Res. Lett.*, 2013, **8**, 81.
13 R. Arppe, T. Näreoja, S. Nylund, L. Mattsson, S. Koho, J. M. Rosenholm, T. Soukka and M. Schäferling, *Nanoscale*, 2014, **6**, 6837.
14 Y. Zhang, N. K. Grady, C. Ayala-Orozco and N. J. Halas, *Nano Lett.*, 2011, **11**, 5519.
15 T. Hanke, J. Cesar, V. Knittel, A. Trügler, U. Hohenester, A. Leitenstorfer and R. Bratschitsch, *Nano Lett.*, 2012, **12**, 992.

 

16 F. P. Bonafé, B. Aradi, M. Guan, O. A. Douglas-Gallardo, C. Lian, S. Meng, T. Frauenheim and C. G. Sánchez, *Nanoscale*, 2017, **9**, 12391.
17 V. Kravtsov, R. Ulbricht, J. M. Atkin and M. B. Raschke, *Nat. Nanotechnol.*, 2016, **11**, 459.
18 J. Ma, Z. Wang and L. W. Wang, *Nat. Commun.*, 2015, **6**, 10107.
19 J. Zuloaga, E. Prodan and P. Nordlander, *ACS Nano*, 2010, **4**, 5269.
20 A. Manjavacas and F. J. Garćia de Abajo, *Nat. Commun.*, 2014, **5**, 3548.
21 J. A. Scholl, A. L. Koh and J. A. Dionne, *Nature*, 2012, **483**, 421.
22 D. C. Marinica, A. K. Kazansky, P. Nordlander, J. Aizpurua and A. G. Borisov, *Nano Lett.*, 2012, **12**, 1333.
23 J. D. Cox, I. Silveiro and F. J. García de Abajo, *ACS Nano*, 2016, **10**, 1995.
24 O. Perez-Gonzalez, N. Zabala, A. G. Borisov, N. J. Halas, P. Nordlander and J. Aizpurua, *Nano Lett.*, 2010, **10**, 3090.
25 P. Song, P. Nordlander and S. W. Gao, *J. Chem. Phys.*, 2011, **134**, 074701.
26 P. Song, S. Meng, P. Nordlander and S. W. Gao, *Phys. Rev. B: Condens. Matter Mater. Phys.*, 2012, **86**, 121410(R).
27 R. Esteban, A. G. Borisov, P. Nordlander and J. Aizpurua, *Nat. Commun.*, 2012, **3**, 825.
28 D. C. Marinica, A. K. Kazansky, H. Lourenco-Martins, J. Aizpurua and A. G. Borisov, *Nano Lett.*, 2013, **13**, 5972.
29 S. Gao, *J. Chem. Phys.*, 2015, **142**, 234701.
30 A. Castro, H. Appel, M. Oliveira, C. A. Rozzi, X. Andrade, F. Lorenzen, M. A. L. Marques, E. K. U. Gross and A. Rubio, *Phys. Status Solidi B*, 2006, **243**, 2465.
31 N. Troullier and J. L. Martins, *Phys. Rev. B: Condens. Matter Mater. Phys.*, 1991, **43**, 1993.
32 G. V. Nazin, X. H. Qiu and W. Ho, *Phys. Rev. Lett.*, 2003, **90**, 216110.
33 J. Yan and S. Gao, *Phys. Rev. B: Condens. Matter Mater. Phys.*, 2008, **78**, 235413.
34 M. T. Sheldon, J. van de Groep, A. M. Brown, A. Polman and H. A. Atwater, *Science*, 2014, **346**, 828.
35 B. N. J. Persson, *Surf. Sci.*, 1993, **281**, 153.
36 A. Hoggard, L. Wang, L. Ma, Y. Fang, G. You, J. Olson, Z. Liu, W. Chang, P. M. Ajayan and S. Link, *ACS Nano*, 2013, **7**, 11209.
37 S. Li and R. R. Jones, *Nat. Commun.*, 2016, **7**, 13405.
38 P. Dombi, A. Hörl, P. Rácz, I. Márton, A. Trügler, J. R. Krenn and U. Hoheneste, *Nano Lett.*, 2013, **13**, 674.
39 M. B. Lien, J. Y. Kim, M. G. Han, Y. C. Chang, Y. C. Chang, H. J. Ferguson, Y. Zhu, A. A. Herzing, J. C. Schotland, N. A. Kotov and T. B. Norris, *ACS Nano*, 2017, **11**, 5925.
40 M. J. Kale, T. Avanesian and P. Christopher, *ACS Catal.*, 2014, **4**, 116.
41 L. Yan, F. Wang and S. Meng, *ACS Nano*, 2016, **10**, 5452.
42 V. Kulkarni, E. Prodan and P. Nordlander, *Nano Lett.*, 2013, **13**, 5873.
43 A. Lauchner, A. E. Schlather, A. Manjavacas, Y. Cui, M. J. McClain, G. J. Stec, F. J. García de Abajo, P. Nordlander and N. J. Halas, *Nano Lett.*, 2015, **15**, 6208.